P-wave Efimov physics implications at unitarity

Yu-Hsin Chen [*]
Department of Physics and Astronomy, Purdue University, West Lafayette, Indiana 47907, USA

Chris H. Greene [†]
Department of Physics and Astronomy, Purdue University, West Lafayette, Indiana 47907, USA
and Purdue Quantum Science and Engineering Institute, Purdue University, West Lafayette, Indiana 47907, USA

(Received 12 September 2022; revised 1 December 2022; accepted 2 March 2023; published 27 March 2023)

Equal mass fermionic trimers with two different spin components near the unitary limit are shown to possess a universal van der Waals bound or resonance state near *s*-wave unitarity, when *p*-wave interactions are included between the particles with equal spin. Our treatment uses a single-channel Lennard-Jones interaction with long-range two-body van der Waals potentials. While it is well known that there is no true Efimov effect that would produce an infinite number of bound states in the unitary limit, we demonstrate that another type of universality emerges for the symmetry $L^{\Pi} = 1^{-}$. The universality is a remnant of Efimov physics that exists in this system at *p*-wave unitarity, and it leads to modified threshold and scaling laws in that limit. Application of our model to the system of three lithium atoms studied experimentally by Du *et al.* [Phys. Rev. Lett. **102**, 250402 (2009)] provides an interpretation of their measured three-body recombination loss rates.

DOI: 10.1103/PhysRevA.107.033329

I. INTRODUCTION

Dilute bosonic and fermionic ultracold gases have benefited tremendously in recent decades from the ability to accurately tune *s*-wave scattering lengths or *p*-wave scattering volumes at two-body Fano-Feshbach resonances [1]. In the most-studied scenario, the *s*-wave scattering length (a_s) between each pair of atoms in a system of three identical bosons diverges to negative infinity and produces the infinite series of trimer bound or resonance state energies in the now-familiar Efimov effect [2–7]. From a hyperspherical coordinate perspective, the Efimov effect occurs because, at two-body unitarity, the long-range adiabatic hyper-radial potential curve is reduced from a repulsive to an attractive asymptotic potential $W(R) \to -(s_0^2 + \frac{1}{4})\hbar^2/(2\mu R^2)$ with $s_0 \approx 1$. Here R is the hyperspherical radius and μ is the three-body reduced mass [8]. Several experimental groups have since demonstrated that the Efimov effect can be observed in helium trimers [9] and in some alkali atom trimers [10–16]. Also, for three identical bosons with orbital angular momentum and parity $L^{\Pi} = 0^{+}$, the scaling of three-body recombination has been predicted and observed [4,17] to vary approximately in proportion to $|a_s|^4$ for negative values of a_s far from resonances.

While the physics of a trimer having *s*-wave interacting particles has been successfully tackled by many different methods, including zero-range models in particular, giving an excellent understanding by now of the Efimov effect with its infinity of bound states at *s*-wave unitarity ($a_s \to \infty$). For equal-mass trimers having *p*-wave interactions, on the other hand, zero-range models have experienced difficulties, leading to predictions of an Efimov effect, e.g., in [18,19], that were ultimately disproven [20], consistent with Refs. [21,22]. Other interesting scenarios that arise with Efimov physics for mass-imbalanced fermionic trimers have been considered by Kartavtsev and Malykh [23] and by Naidon *et al.* [24], but our focus here is exclusively on equal-mass trimers. In equal-mass two-component trimers and in spin-polarized fermionic trimers, there are no known symmetries having an Efimov effect at *s*-wave or *p*-wave unitarity. The point of the present study is to show that properties of fermionic trimers can be reliably predicted using realistic finite-range potentials relevant to current ultracold atomic physics experiments. Our treatment addresses two main goals: Firstly, (i) We show that despite the absence of an Efimov *effect* in fermionic trimers with *p*-wave interactions, there is a remnant of Efimov *physics* in the sense described in other recent references [22,25], namely, that going to *s*-wave unitarity and/or *p*-wave unitarity produces a reduction of the long-range hyper-radial potential barrier. This reduction results in modifications of recombination threshold laws and scalings versus scattering length and volume. Secondly, (ii) We apply our model to an experimental measurement of three-body recombination in a two-component Fermi gas near unitarity [26] that has gone more than a decade without any theoretical interpretation. Our treatment shows that the basic physics observed in that measurement can at last be understood in the framework presented here.

The scaling law of two-component equal-mass fermionic three-body recombination rate was predicted by D'Incao and Esry to be $|a_s|^{2.455}$ for $a_s < 0$ [27], as well as by D'Incao and Petrov to be a_s^6 for $a_s > 0$ [27,28]. For the negative a_s side, the scaling law of three-body recombination (K_3)

[*]chen2662@purdue.edu
[†]chgreene@purdue.edu

disagrees significantly with the experimental result that was observed, $K_3 \propto |a_s|^{0.79\pm0.14}$ for $a_s < 0$ [26]. One point about this theory-experiment discrepancy, which is relevant to the present study, is that those previous theoretical predictions neglect the interaction between the two spin-up fermions, which might potentially be responsible for the discrepancy in the threshold law compared to the experimental results. However, the experimental temperature was too high [26] for the theoretical threshold law scaling to apply.

The present article predicts the existence of one p-wave universal trimer state for two-component equal-mass ($m_\uparrow = m_\downarrow$) fermionic trimers having the s-wave scattering length approaching infinity between spin-up and spin-down fermions and having the p-wave scattering volume (V_p) at the unitary limit, for the symmetry $L^\Pi = 1^-$. Evidence for the universality of this trimer state has emerged from our tests of different s- and/or p-wave poles of two-body Lennard-Jones potentials, in addition to various other two-body potentials, e.g., Gaussian or Gaussian-type potentials [22,25]. The peak of the three-body recombination rate indicates the point where the trimer state becomes bound. The scaling law for the three-body recombination rate as a function of the p-wave scattering volume V_p is modified when the opposite-spin fermion interactions are at or near s-wave unitarity. For a two-component Fermi gas trimer, especially the two spin-up and one spin-down fermion case, the symmetry $L^\Pi = 1^-$ dominates near the three-body dissociation threshold, because the recombination rate linearly on the collision energy E [29]. However, $K_3 \propto E$ no longer applies at the s-wave or p-wave unitary limit for the opposite spin fermions, or if the two spin-up fermions interact at p-wave unitarity. The calculations presented here also overcome a longstanding inability of theory to understand the recombination rate measured in an experiment [26] carried out at very large s-wave scattering lengths. We do not argue, however, that this approximate agreement between theory and experiment can be viewed as a confirmation of the universal trimer discussed above.

II. METHOD

The adiabatic hyperspherical representation describes few-body interactions and collisional phenomena [5,7,30,31] and is applied here to the three-body quantum problem. The two spin-up fermions interact with one spin-down fermion (or any other equal-mass particle) with symmetry $L^\Pi = 1^-$, where Π is the total parity. The three-body Schrödinger equation is rewritten using modified Smith-Whitten hyperspherical coordinates [8,32–34]:

$$\left[-\frac{\hbar^2}{2\mu}\frac{d^2}{dR^2} + W_\nu(R)\right]F_\nu(R) + \sum_{\nu\neq\nu'} W_{\nu\nu'}F_{\nu'}(R) = EF_\nu(R). \tag{1}$$

Here R is the hyperspherical radius, $\mu = m/\sqrt{3}$ is the three-body reduced mass for three equal particles with mass m, $W_\nu(R)$ is the effective *adiabatic potential* in channel ν obtained from the hyperangular eigenvalue equation, $F_\nu(R)$ is the hyper-radial wave function, and $W_{\nu\nu'}(R)$ is the nonadiabatic coupling. The full interaction potential energy V is taken here to be a sum of the two-body potentials, i.e., $V = v_3(r_{12}) + v_1(r_{23}) + v_2(r_{31})$, where the r_{ij} are the interparticle distances. The two-body potential utilized is the Lennard-Jones potential [35],

$$v_i(r) = -\frac{C_6}{r^6}\left(1 - \frac{\lambda_n^6}{r^6}\right). \tag{2}$$

In this paper, in our chosen set of van der Waals units, the C_6 coefficient is set at $16\,r_{\rm vdW}^6 E_{\rm vdW}$, where $r_{\rm vdW}$ is the van der Waals length $r_{\rm vdW} \equiv (mC_6/\hbar^2)^{1/4}/2$ ($m/2$ is two-body reduced mass here) and the van der Waals energy unit is $E_{\rm vdW} \equiv \hbar^2/(2\mu r_{\rm vdW}^2)$. The parameter λ_n can be adjusted to produce any desired s-wave scattering length or p-wave scattering volume for a chosen pair of fermions. Here the two-body s-wave scattering length and p-wave scattering volume can be written at $k \to 0$ as

$$k^{2\ell+1}\cot(\delta_\ell) \to -1/{a_\ell}^{2\ell+1} + \tfrac{1}{2}r_\ell k^2, \tag{3}$$

where $a_0(\equiv a_s)$ is the s-wave scattering length, $a_1(\equiv a_p)$ is the p-wave scattering length, $\delta_0(k)$ is the s-wave scattering phase shift, $\delta_1(k)$ is the p-wave scattering phase shift, r_0 is the s-wave effective range, r_1 is the p-wave "effective range," and k is the wave number.

The asymptotic effective adiabatic potentials in the three-body continuum are accurately characterized at $R \to \infty$ as

$$W_\nu(R) \to \frac{\hbar^2 l_e(l_e+1)}{2\mu R^2}, \tag{4}$$

where l_e controls the effective angular momentum barrier of the three free asymptotic particles in the large hyperradius, $R \to \infty$. The l_e value also determines the scaling law of the three-body recombination rate and squared scattering matrix element, through the Wigner threshold law $|S^{L\Pi}_{j\leftarrow i}|^2 \propto {k_i}^{2l_{e,i}+1}$. R-matrix propagation is used to solve the radial Eq. (1), and the three-body recombination rate ($K_3^{L\Pi}$) can be computed in terms of the scattering S matrix as

$$K_3^{L\Pi} = \sum_{L,\Pi}\sum_{i,j}\frac{32\hbar N!(2L+1)}{\mu k^4}\left|S^{L\Pi}_{j\leftarrow i}\right|^2. \tag{5}$$

Here N is the number of identical particles in the trimer, $k = \sqrt{2\mu E/\hbar^2}$ is the hyperspherical wave number, E is the three-body collision energy, and i and j label the incident (three-body continuum) and outgoing (three-body recombination) channels attached to two-body energies [36,37]. The situation with two spin-up and one spin-down fermion can be viewed as two identical fermions plus a third atom of equal mass, in which case $N = 2$ in Eq. (5). According to the Wigner threshold law, the three-body recombination rate is a power-law function of $k = \sqrt{2\mu E/\hbar^2}$ at ultracold energy, namely,

$$K_3^{L\Pi} \propto k^{2l_e-3}. \tag{6}$$

Therefore the coefficient of $1/(2\mu R^2)$ in the asymptotically lowest continuum effective adiabatic potential plays a key role in the behavior of the low-energy three-body recombination rate.

III. *P*-WAVE UNIVERSAL TRIMER

Our explorations demonstrate the existence of a p-wave universal trimer for three equal-mass fermionic atoms at the

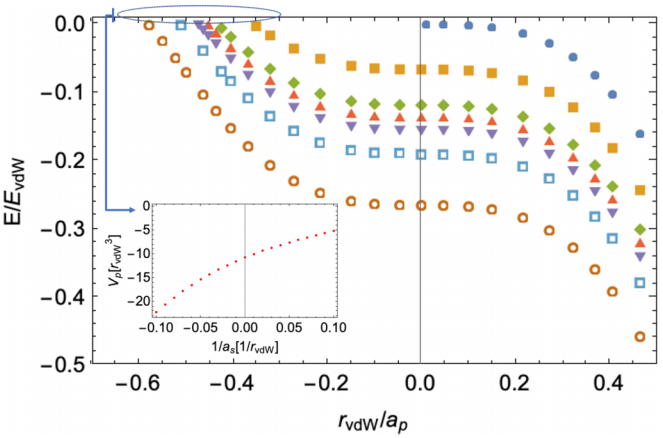

FIG. 1. Shown are p-wave universal trimer state energies for two spin-up and one spin-down fermion systems ($\uparrow\downarrow\uparrow$) with vs the inverse of p-wave scattering length ($a_p \equiv V_p^{1/3}$). Circles (solid blue) show the two-body p-wave bound state. The squares, diamonds, triangles, inverted triangles, open squares, and open circles represent, respectively, the trimer energies obtained using different fixed interactions (scattering lengths) between the spin-up and spin-down fermions ($\uparrow\downarrow$) plotted here as functions of the p wave a_p between the two spin-up fermions ($\uparrow\uparrow$). The respective s-wave values of a_s in the order listed above for the different symbols are $a_s = -10\, r_{\rm vdW}$, $a_s = -50\, r_{\rm vdW}$, $a_s = \infty\, r_{\rm vdW}$, $a_s = 50\, r_{\rm vdW}$, $a_s = 20\, r_{\rm vdW}$, and $a_s = 10\, r_{\rm vdW}$. The inset figure shows the starting value of a_p, where two spin-up and one spin-down fermion first form the trimer state at zero energy for the corresponding value of the s-wave scattering length between opposite-spin-state fermions.

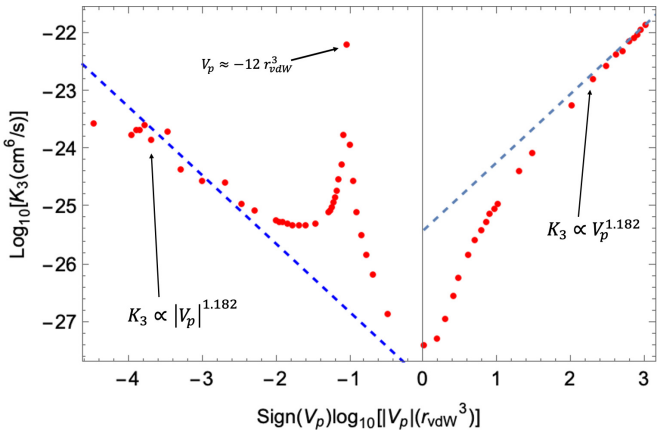

FIG. 2. Our numerically computed three-body recombination rate is shown as a function of the p-wave scattering volume V_p for the symmetry $L^\Pi = 1^-$. The interaction between opposite spin fermions is fixed at unitarity. This plot represents the three ^{6}Li atoms with two spin-up and one spin-down state ($\uparrow\downarrow\uparrow$) at the temperature $E/k_B \approx 150$ nK. The peak of the recombination rate at $V_p \approx -12\, r_{\rm vdW}^3$ is close to the previously discussed starting point where the universal trimer first becomes bound, near the first p-wave pole of two-body Lennard-Jones potential. Moreover, the dashed line asymptote shows the expected scaling law of the recombination rate for the computed value of l_e, namely, for this symmetry $K_3 \propto |V_p|^{1.182}$. The x and y axis are both logarithmic scales, base 10.

s-wave unitary limit, which emerges when the interaction between the two spin-up atoms is made attractive, specifically for the symmetry $L^\Pi = 1^-$. Figure 1 plots the p-wave trimer state energy versus the p-wave scattering length ($a_p \equiv V_p^{1/3}$) between the identical fermions; this was calculated by including 30 coupled continuum channel potential curves. Different symbols represent the different s-wave scattering lengths between the opposite-spin-state fermions. As one increases the attraction in the p-wave potential between spin-polarized fermion, it is seen that the trimer can be created not only at the s-wave unitary limit for the opposite-spin fermion interactions, but even at small positive or negative values of the s-wave scattering length.

In the case where the unequal spin interactions are fixed at s-wave unitarity and the interactions between like fermions are at p-wave unitarity, the universal trimer energy is computed here to equal $E = -0.136\, E_{\rm vdW}$, where the two-body s-wave and p-wave effective ranges are $r_s \approx 2.782\, r_{\rm vdW}$ and $r_p \approx -1.727\, r_{\rm vdW}^{-1}$, respectively. The resonance energies, when different spin fermions interact at the first s-wave pole and two spin-up fermions are at either the second or third p-wave pole, are both $E = -0.129\, E_{\rm vdW}$. The critical points where the universal trimer state reaches zero energy and causes a recombination resonance can be determined from the axis intercepts in Fig. 1. The inset of Fig. 1 shows those critical values of V_p as a function of a_s, as the s-wave scattering length ranges from $-10\, r_{\rm vdW}$ to ∞ and on to $10\, r_{\rm vdW}$. For this a_s regime, there is no additional p-wave two-body resonance, nor has a p-wave Feshbach molecule been created. The inset figure suggests how experiment can find the recombination resonance associated with the universal trimer state, when the different spin fermion interactions differ from the s-wave unitary limit.

IV. MODIFIED WIGNER THRESHOLD LAW AT UNITARITY

Measuring the three-body recombination rate gives a way to find values of the two-body scattering parameters where the universal trimer state hits zero energy. Consider next the situation where unlike spins have their interaction fixed at s-wave unitarity, as the p-wave scattering volume V_p is varied between the same spin fermions. Figure 2 plots the three-body recombination rate versus V_p for two spin-up and one spin-down ($\uparrow\downarrow\uparrow$) ^{6}Li atom with symmetry $L^\Pi = 1^-$. The resonant peak of the recombination rate corresponds to the creation of the universal trimer state, predicted here to occur when the p-wave scattering volume is $V_p \approx -12\, r_{\rm vdW}^3$. This recombination rate was calculated by including six atom-dimer channels for recombination channels and 14 continuum channels. This V_p is close to its value predicted in our inset of Fig. 1, $V_p \approx -11.06\, r_{\rm vdW}^3$ (including 14 continuum channels and no atom-dimer channels). The slight difference between the resonant value of V_p in our true bound state and scattering calculations arises because the number of fragmentation channels is different in these two calculations that are so different. In one case the state of interest is a bound state extrapolated to zero energy, while in the latter case it is a resonance in the predissociative continuum. Still, the difference gives some insight into the size of expected departures from universality. Note the dramatic dependence on V_p: the peak value of K_3

being around five orders of magnitude higher than the K_3 value at zero p-wave scattering volume. The asymptotic behavior of the recombination rate K_3, for $|V_p| \gg r_{vdW}^3$, has been modified to $|V_p|^{(2l_e+1)/3} \to |V_p|^{1.181}$ since the value of l_e controlling the large-R adiabatic potential is modified to $l_e = 1.272$ by Efimov physics for the two-component fermion system in the s-wave unitary limit.

The Efimov physics modification [22,25], for this two-component Fermi trimer at s-wave unitarity in the symmetry $L^\Pi = 1^-$, can be obtained by solving the transcendental equation for zero-range interactions, as in Refs. [38,39]. We confirm numerically that the lowest l_e value, which sets the long-range barrier of the three-body effective potential, controls both the Wigner threshold law Eq. (6) and the scaling of the three-body recombination rate with the p-wave scattering volume. In the bosonic Efimov effect, there are an infinite number of Stückelberg minima occurring as a_s grows arbitrarily large and positive. However, there is no true Efimov effect in the present fermionic case; thus the phase difference between pathways does not necessarily complete even a single full cycle, as V_p is varied over the range plotted in Fig. 2. There is no Stückelberg minimum in the range we have considered, but one would be expected if the recombination rate were computed to much higher energies.

V. THREE-BODY LOSS RATE OF A TWO-COMPONENT FERMIONIC TRIMER AT S-WAVE UNITARITY

In this section the three-body recombination K_3 are calculated and discussed by adding the p-wave interaction between two spin-up fermions while the opposite-spin-state fermion is close to s-wave unitarity with $L^\Pi = 1^-$. The detail of reason of the loss rate increasing when s-wave scattering from small negative to negative infinite, then from positive infinite to small positive, will be discussed in the following sections.

A. Three-body loss rate compared with experiment

The thermally averaged three-body recombination rate is written (after correcting a typo in Eq. (4) of Ref. [40]) as

$$\langle K_3\rangle(T) = \frac{1}{2(k_B T)^3}\int K_3(E)E^2 e^{-E/(k_B T)}dE. \qquad (7)$$

Our computed recombination rate shows rough agreement with the ternary loss rate measurement carried out by the group of Thomas [26] for a two-component gas of fermionic ^{6}Li. Figure 3 compares theory and experiment in a plot of the thermally averaged *atom-loss* rate $\langle L_3\rangle(T)$. This quantity is related to the event loss rate K_3 through the equation $\langle L_3\rangle(T) = 3\langle K_3\rangle(T)/2$ [17], where the brackets denote thermal averaging. The computed results in Fig. 3 are for the recombination of two spin-up and one spin-down ^{6}Li atom in the symmetry $L^\Pi = 1^-$ and are shown as a function of $r_{\rm vdW}/a_s$, which controls the interaction of opposite-spin-state fermions. Moreover, the p-wave scattering volume between two spin-up fermions has been fixed [41] at $V_p \approx -1.8\, r_{\rm vdW}^3$. For two ^{6}Li atoms, the van der Waals length is equal to $r_{\rm vdW} = 31.26\, a_B$ and the van der Waals energy is $E_{\rm vdW}/k_B = 29.47$ mK, where a_B and k_B are the Bohr radius and the Boltzmann constant, respectively [42]. The open circles were calculated using the

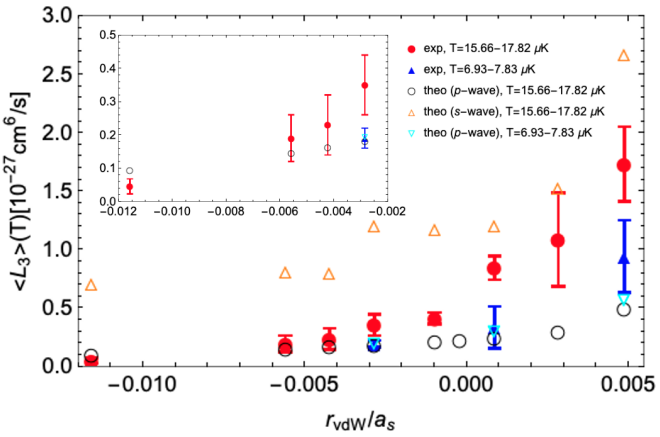

FIG. 3. Comparison of the theoretical thermally averaged three-body loss rate for ^{6}Li with the Du *et al.* experiment [26] at large scattering length $|a_s|$ using the two spin-up and one spin-down ($\uparrow\downarrow\uparrow$) model with trimer orbital angular momentum $L^\Pi = 1^-$, and the temperature range is from $T \approx 15.66\,\mu$K to $T \approx 17.82\,\mu$K. The filled circles (red) represent the experimental data from $T \approx 15.66\,\mu$K to $T \approx 17.82\,\mu$K, and the filled triangles (blue) are the experimental data at lower temperature from $T \approx 6.93\,\mu$K to $T \approx 7.83\,\mu$K. The open circles (black), open triangles (orange), and inverted triangles (cyan) are our numerical calculations of the thermally averaged three-body loss rate for two different Hamiltonians, as explained in the text.

three-body Born-Oppenheimer potential curves obtained for a Hamiltonian that includes deep p- and f-wave atom-dimer recombination channels only, and the inverted triangles were obtained using the same potential curves but at lower temperature to make comparison with experimental data. The open triangles were calculated instead for a Hamiltonian that possesses deep atom-dimer recombination channels, from s wave to g wave.

Our study concentrates on the recombination into deep atom-dimer channels for the recombination process; recombination into the shallow s-wave atom-dimer channel at large positive values of the s-wave scattering length is omitted from the theoretical results shown in Fig. 3 because of the extremely small binding energy of those universal dimers for the positive scattering lengths used in that experiment, with binding energies smaller than the trapping potential and the gas temperature. A recombination event thus does not eject any atoms from the trap, and also the dimer will be dissociated rather quickly after it is formed. Parenthetically, we note that if recombination into the weakly bound universal s-wave dimer is included, the recombination would be a_s^6 for $a_s > 0$ [27,28] and the rate would be several orders of magnitude higher than the largest experimental rate shown in Fig. 3, but this is not our justification for omitting those from our calculated rate to compare with experiment.

In Fig. 3 the (red) circles represent the experimental three-body loss rate coefficient as a function of the s-wave scattering length (a_s) which is taken from Table I of Ref. [26], with a_s rescaled into units of the van der Waals length. The triangles (blue) show the experimental three-body atom loss rate at lower temperatures. The calculations omit recombination into the weakly bound universal s-wave dimer; the p-wave theory

TABLE I. Shown are the s-wave and p-wave effective ranges (second and fourth row) with respective to s-wave scattering length and p-wave scattering volume, which are associated with Fig. 3. The a_s are s-wave scattering lengths between spin-up and spin-down fermions, and the V_p is p-wave scattering volume within two spin-up fermions with angular momentum $L^{\Pi} = 1^-$.

a_s ($r_{\rm vdW}$)	−86.37	−179.14	−236.72	−351.89	−1023.67	1151.63	351.89	204.73
s-wave $r_{\rm eff}$ ($r_{\rm vdW}$)	2.85	2.82	2.81	2.80	2.79	2.78	2.77	2.76
V_p ($r_{\rm vdW}^3$)				−1.8				
p-wave $r_{\rm eff}$ ($r_{\rm vdW}^{-1}$)				44.43				

gives reasonable agreement with the two points on the positive $1/a_s$ side (agreeing better at the lower temperature measured). For our model that only includes recombination into deep s-wave dimers, there is one point close to the experimental result at higher temperature, but this agreement could be fortuitous. Table I shows the s- and p-wave effective ranges corresponding to the situation of Fig. 3; the s-wave effective range was calculated by using the method from Ref. [43].

B. Born-Oppenheimer potential curves

The lowest several hyperspherical Born-Oppenheimer potential curves for the three-fermion system with symmetry $L^{\Pi} = 1^-$ are shown in Fig. 4, which enables an interpretation of the difference between the three-body loss rates computed using the two different Hamiltonians described in relation to Fig. 3 of the main text. The long-range effective adiabatic potential curve representing the highest atom-dimer channel can be represented asymptotically as

$$W_\nu(R) \xrightarrow[R\to\infty]{} U_\nu(R) = E_{\nu l} + \frac{\hbar^2 l'(l'+1)}{2\mu R^2}. \tag{8}$$

Here $E_{\nu l}$ is the rovibrational dimer energy, l represents the dimer angular momentum, and l' is the angular momentum of the third particle relative to the dimer. For the three-body hyperspherical calculations shown in Figs. 4(a) and 4(b), the s-wave two-body potential depth has been chosen to yield the stated values of the scattering lengths (a_s) between spin-up and spin-down fermions, in the vicinity of the second s-wave pole (i.e., there exists a single deep s-wave dimer, in addition to deep $p, d, f,$ and g dimers, plus a weakly bound s-wave dimer when $a_s > 0$), while the p-wave scattering volume between two spin-up fermions was set at $V_p = -1.8\, r_{\rm vdW}^3$ (no p-wave dimer exists in this two-body potential).

The insets show that the potential barrier exhibits a local maximum (at $R \approx 5\, r_{\rm vdW}$) in the entrance recombination channel, and tunneling through that barrier to reach smaller hyper-radii plays a key role in determining the experimental three-fermion recombination loss rate into an atom and a deep dimer. The barrier decreases gradually as the s-wave scattering length is decreased from a small negative value to $-\infty$ and as a_s continues to decrease from $+\infty$ to small positive values ($a_s = -86 \to \infty \to 205\, r_{\rm vdW}$), i.e., as the interaction potential between opposite spin fermions gets increasingly attractive. Since three-body recombination into deep dimers in this low energy range requires the system to tunnel through that barrier, the gradual decrease of that hyper-radial barrier height, as the opposite spin dimer interaction gets more attractive, produces an enhancement of the partial three-body recombination rate.

Similar reasoning applies to the other two figures, Figs. 4(c) and 4(d), the only differences being that: (i) the s-wave interaction between opposite-spin-state fermions has been chosen near the first s-wave pole and (ii) the p-wave interaction between same-spin-state fermions is still fixed at $V_p = -1.8\, r_{\rm vdW}^3$ but with a deeper vdW potential that supports both deep p-wave and f-wave bound states. Interestingly, one sees that the computed hyper-radial barrier heights in the entrance channels of Figs. 4(c) and 4(d) are about 30% higher than those plotted in Figs. 4(a) and 4(b).

Observe that the open circle recombination rate calculation shown in Fig. 3 involves an s-wave scattering length a_s between opposite-spin-state fermions that was computed at or near the first s-wave pole and where only the two spin-up fermion can form deep dimers of p-wave and f-wave angular momentum. In this case, the more weakly bound f-wave deep dimer partial recombination rates are computed to be slightly higher than the p-wave partial recombination rates. The relevant hyper-radial Born-Oppenheimer potentials for those cases, with $a_s = -86\, r_{\rm vdW}$ and $a_s = 205\, r_{\rm vdW}$, are those displayed in Figs. 4(c) and Fig. 4(d), respectively.

VI. WIGNER THRESHOLD LAW IN TWO-COMPONENT FERMION AT UNITARITY

The Wigner threshold law for the three-body recombination in a low energy collision of two spin-up and one spin-down fermion with symmetry $L^{\Pi} = 1^-$ is $K_3(E) \propto E$ [29], for interactions not at unitarity. The power law of the three-body recombination depends on the number of identical particles and the system's angular momentum. However, when the two-body interaction is strong enough, i.e., the two-fermion interactions reside at the s-wave or p-wave unitary limit, the power law of the recombination becomes modified because there is a modified centrifugal barrier asymptotically. In particular, the asymptotic l_e value of the lowest three-body continuum channel changes at unitarity, in a remnant of the Efimov effect [22,25]. Figure 5 shows that in the very-low-energy limit, the threshold law of the three-body recombination rate into deep dimers does exhibit the expected linear dependence on the energy, $K_3(E) \propto E$, for collision energies from $0.03\,\mu K$ to $1\,\mu K$. However, the figure documents that the power law dependence of the recombination rate changes to $K_3(E) \propto E^{-0.227}$ when the temperature is in the range from $10\,\mu$K to $10^4\,\mu$K. The main point is that while there is no true "Efimov effect" in this case, there is still the Efimov physics reduction of the coefficient l_e which is reduced by Efimov physics in the s-wave unitarity regime to 1.272 from its noninteracting value of 5/2. This controls the energy dependence of the recombination rate, which varies as $E^{l_e - 3/2} = E^{-0.227}$, and this scaling is shown in Fig. 5 to

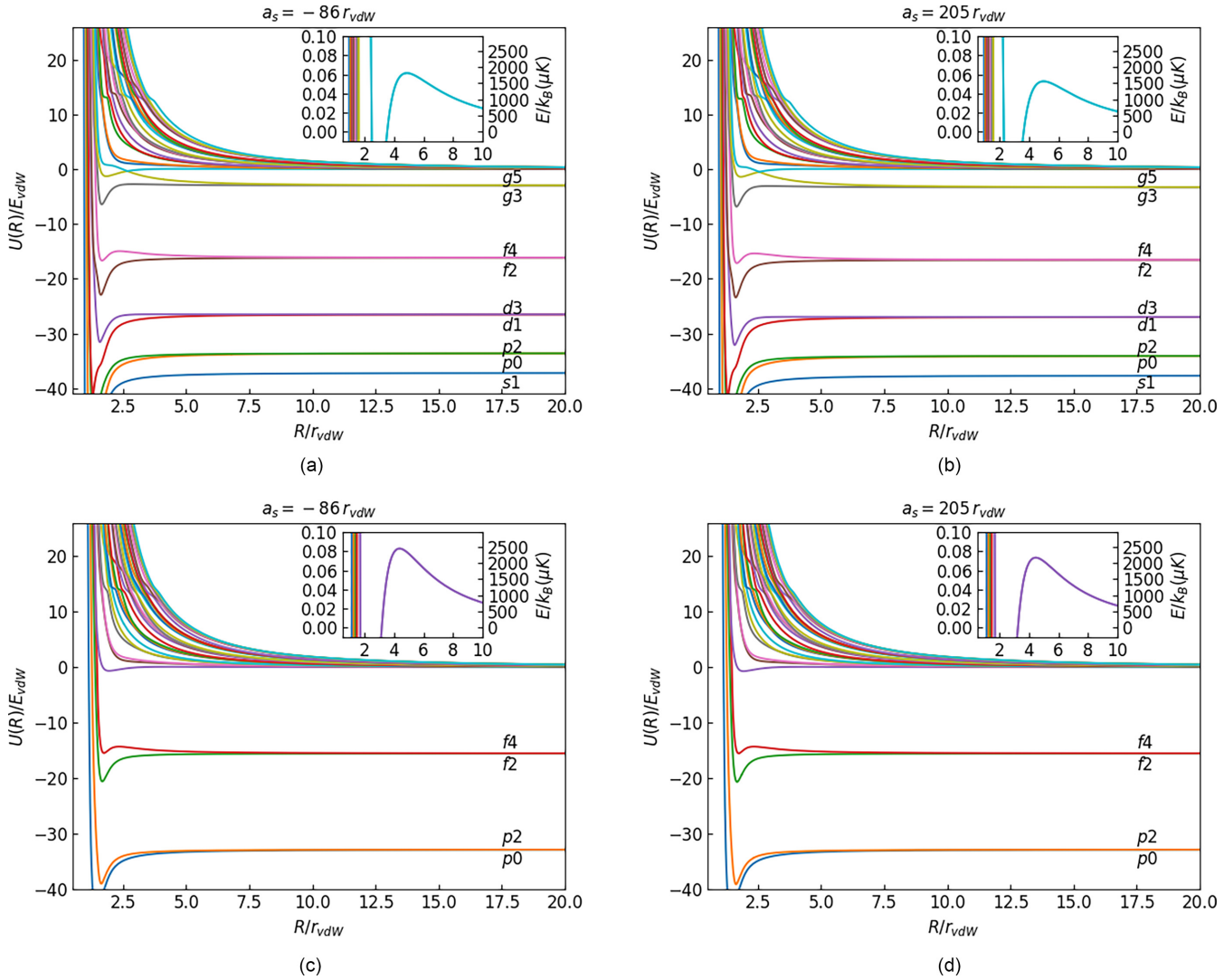

FIG. 4. Three-body Born-Oppenheimer potential curves for two spin-up and one spin-down fermion ($\uparrow\downarrow\uparrow$) with total angular momentum $L^{\Pi} = 1^{-}$. The letter represents the angular momentum quantum number l of the dimer, and the number labels the angular momentum between the third atom and dimer l'. (a, b) The a_s are chosen near the second s-wave pole with one deep s-wave bound state, and $V_p = -1.8\, r_{\rm vdW}^3$ with no p-wave bound state. In (c) and (d), the a_s are chosen near or at the first s-wave pole with no deep opposite spin dimers, and the potential producing $V_p = -1.8\, r_{\rm vdW}^3$ is chosen to have deep p- and f-wave bound states that enable recombination into deep spin-polarized dimers.

hold from approximately 10 μK up to about 10 mK (see the red dashed line in Fig. 5). If there were no Efimov physics reduction of the coefficient l_e controlling the long range hyperradial potential curve, the energy dependence would be much different, namely, K_3 proportional to E. The inset of Fig. 5 displays a WKB calculation to analyze the threshold law of the three-body recombination loss rate. The WKB tunneling probability at the incident energy E can be written as [7]

$$P_{x\to y}^{(\nu)} = \exp\left\{-2\int_x^y \sqrt{\frac{2\mu}{\hbar^2}\left[W_\nu(R) - E + \frac{1/4}{2\mu R^2}\hbar^2\right]}dR\right\}, \tag{9}$$

where the ν represents the νth channel, and x and y are the inner and outer classical turning points, respectively. Here E is the incident collision energy and $\hbar^2(1/4)/(2\mu R^2)$ is the semiclassical Langer correction [44]. The inset of Fig. 5 shows that the WKB probability has been raised to the power $1/1.773$ and plotted versus the energy. The demonstrated proportionality between $P(E)$ and $E^{1.773}$ clarifies why the three-body recombination rate into deep dimers has this nonstandard (Efimov physics modified Wigner threshold law) in its near-threshold behavior at large s-wave scattering lengths.

VII. LANDAU-ZENER PROBABILITY

If these adiabatic potential curves and their nonadiabatic couplings are computed out to very large hyper-radii ($R \gg 10a_s$), one could simply solve the coupled one-dimensional differential equations to obtain the full scattering matrix of the system. That is impractical here for $a_s > 0$ because there is a crucial avoided crossing between the two potentials sketched in Fig. 7 out at huge hyper-radii that are beyond our current computational capabilities. However, we understand that the nonadiabatic coupling of those two channels can be

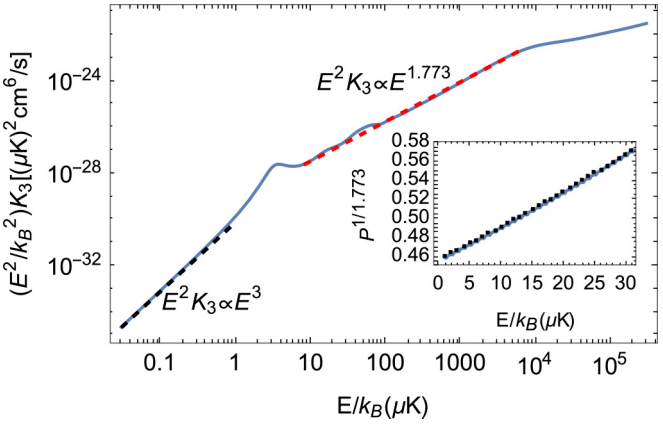

FIG. 5. Shown here is the rescaled recombination rate, $E^2K_3(E)$, as a function of the total energy E. The interaction between opposite-spin-state fermions ($\uparrow\downarrow$) is set at $a_s = 205\, r_{\rm vdW}$ and the interaction between the two spin-up fermions ($\uparrow\uparrow$) is equal to $V_p = -1.8\, r_{\rm vdW}^3$, corresponding to the three-body potential curves that are shown in Fig. 4(d). The inset confirms that the power law for the WKB tunneling probability varies linearly with collision energy at very low energy, consistent with the expected Wigner threshold law for this symmetry.

approximately modeled as a Landau-Zener avoided crossing. The nonadiabatic coupling matrices $P_{\nu\nu'}(R)$ and $Q_{\nu\nu'}(R)$ are defined as

$$P_{\nu\nu'}(R) = \int d\Omega \Phi_\nu^*(R;\Omega)\frac{\partial}{\partial R}\Phi_{\nu'}(R;\Omega), \tag{10}$$

$$Q_{\nu\nu'}(R) = \int d\Omega \Phi_\nu^*(R;\Omega)\frac{\partial^2}{\partial R^2}\Phi_{\nu'}(R;\Omega). \tag{11}$$

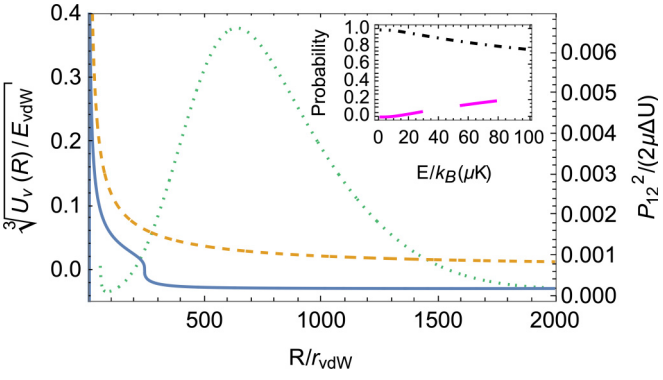

FIG. 6. The lowest two Born-Oppenheimer potential curves calculated near the first s- and p-wave poles are shown for symmetry $L^\Pi = 1^-$. The interaction between the spin-up and spin-down fermions is set at $a_s = 205\, r_{\rm vdW}$ and between the two spin-up fermions at $V_p = -1.8\, r_{\rm vdW}^3$. The solid line decreases below the three-body continuum threshold at around $R = 240\, r_{\rm vdW}$, while the dashed line is the lowest continuum channel potential curve, and the dotted line is a measure of the nonadiabatic coupling strength, showing a peak located near $R = 619\, r_{\rm vdW}$. The inset plots the Landau-Zener probability as a function of the collision energy. Specifically, the dash-dotted line (black) denotes the diabatic probability, and the long-dashed line (magenta) is the adiabatic probability.

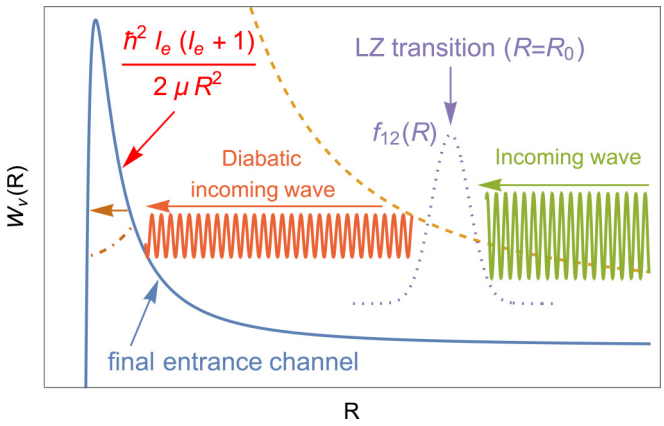

FIG. 7. Sketch of the Landau-Zener transition between the two lowest Born-Oppenheimer potential curves at the large positive a_s, where the l_e value of the lower potential curve plays a key role in controlling the low-energy-threshold behavior of the three-body recombination rate. The solid curve is the lowest potential curve, which effectively acts as the three-body entrance channel at $R < R_0$, even though it goes below the three-body threshold and becomes an atom-dimer channel at very large $R \gg a_s$. The dashed curve plots the second lowest potential curve that becomes the second continuum channel at $R < R_0$ and which serves as the lowest three-body continuum entrance channel at $R \gg R_0$. The dotted line shows the measure of nonadiabatic coupling strength $f_{12}(R)$ and its peak position that is concentrated at $R = R_0$.

The following quantity serves as a useful measure of the nonadiabatic coupling strength between channels ν and ν':

$$f_{\nu\nu'}(R) = \frac{P_{\nu\nu'}(R)^2}{2\mu|U_\nu(R) - U_{\nu'}(R)|}. \tag{12}$$

Figure 6 plots the cube root of the lowest two Born-Oppenheimer potential curves as a function of hyperradius and compares it with the nonadiabatic coupling strength. The solid curve (s-wave atom-dimer channels) goes below the three-body threshold at around $R = 240\, r_{\rm vdW}$ and converges asymptotically to the universal dimer energy appropriate to a large positive a_s. The dashed curve is the lowest three-body continuum channel that converges to 0 asymptotically, and the dotted curve represents the measure of nonadiabatic coupling strength $f_{12}(R)$ between these two channels. The peak of the nonadiabatic coupling means the three-body system has a high chance to cross diabatically as it moves inward from the continuum channel to the atom-dimer channel near the hyperradius $R \approx 3a_s$. The inset of Fig. 6 shows the Landau-Zener transition probability versus the collision energy. The Landau-Zener probability to diabatically traverse an avoided crossing centered at the hyperradius R_0 can be represented as [45]

$$P_{\rm diabatic} = \exp\left\{\frac{-2\pi U_{12}^2}{\hbar v|\frac{\partial}{\partial R}[U_1(R) - U_2(R)]|}\right\}, \tag{13}$$

where $U_1(R)$ and $U_2(R)$ are the two hyperspherical potential curves, v is the semiclassical local hyper-radial velocity, the minimum potential energy gap is $U_{12} = U_1(R_0) - U_2(R_0)$, and the slope difference in the denominator of the exponent is computed near but not exactly at R_0. In the inset, the

Landau-Zener diabatic probability is seen to be close to unity in this low energy range, namely, $P_{\text{diabatic}} = 0.977$, with the transition centered at $R = 619\, r_{\text{vdW}}$ for the energy $E \approx 15.66\, \mu$K in the range of energy and s-wave scattering length relevant for the experiment [26]. Note that the three-body recombination loss rate in Fig. 3 has incorporated this diabatic probability factor from the Landau-Zener transition for the calculations performed at large positive s-wave scattering lengths. Figure 7 illustrates the mechanism of the Landau-Zener transition between the two lowest potential curves, and the l_e value of lowest potential curve has a significant effect on the threshold law of the three-body recombination rate.

One subtlety in our present calculations that requires explanation is the fact that for the large positive scattering lengths studied experimentally (in Fig. 3 of the main article), there is a very weakly bound s-wave dimer of binding energy below 1 μK. Recombination into that dimer is not expected to result in atom loss. For positive a_s, therefore, the lowest energy *true* three-body entrance channel is the dashed curve shown in Fig. 7. However, in order to reach small hyper-radii where recombination into deep dimers can occur, the system must reach the region left of the potential barrier of the solid (blue) potential curve in Fig. 7. Because the two potential curves in the figure have an avoided crossing at $R_0 \approx 3a_s$, this provides a dominant pathway for recombination into deep dimers that involves the incoming three-body wave that transitions nonadiabatically into the solid potential curve labeled as the final entrance channel and can then tunnel to the left of the potential barrier where recombination subsequently occurs.

This sequence of steps that control deep dimer formation in such a collision has apparently not been described in previous studies of three-body recombination. Since $a_s \gg r_{\text{vdW}}$ in the range considered here, the solid (blue) potential curve in Fig. 7 is the one that has its l_e value affected strongly by Efimov physics, and for $R_{\text{barrier}} \ll R \lesssim a_s$ it is reasonably well described by a centrifugal barrier whose coefficient is $l_e(l_e+1)$ with $l_e \approx 1.273$. The tunneling amplitude through that barrier has an energy dependence described by an Efimov-modified Wigner threshold law factor $k^{l_e+1/2}$, as has been stressed in recent publications [22,25]. Thus the three-body recombination rate has the following energy dependence: $K_3 \propto E^{l_e-3/2} = E^{-0.227}$, over the energy range from about 10 μK up to 5 mK, and the WKB tunneling probability varies with energy as $P \propto E^{l_e+1/2} = E^{1.773}$, respectively (i.e., the exponent is 2–0.227). Previous studies have shown how WKB tunneling under such a centrifugal barrier is one way of understanding the origin of the relevant Wigner threshold law for any given process [46]. Therefore the numerical thermally averaged three-body loss rate into deep dimer formation can be described for large positive a_s in terms of this pathway that involves the Landau-Zener transition probability followed by tunneling. This reasoning is not relevant at large negative a_s, because in that case the solid (blue) curve of Fig. 7 remains positive all the way out to $R \to \infty$ and consequently behaves just as a normal three-body entrance channel, albeit with an Efimov-physics modified value of its centrifugal barrier equal to $l_e \approx 1.273$ out to $R \lesssim |a_s|$ (see Refs. [22,25]).

VIII. CONCLUSION

In summary, the Fermi gas with equal-mass atoms in two spin components has been shown to support a universal trimer that can be created by tuning the s-wave and p-wave interaction simultaneously, and this trimer produces an observable resonance in the three-body recombination rate. Moreover, the scaling law of the three-body recombination rate as a function of p-wave scattering volume is shown to be modified when the pair of spin-up and spin-down fermions near interacts at the s-wave unitary limit. The three-body inelastic collision rates have been computed as a function of the s-wave scattering length, with the interaction between the two equal spin fermionic lithium atoms included, and it provides a reasonable interpretation of the recombination rates measured by Du *et al.*

ACKNOWLEDGMENTS

This work was supported in part by NSF Grant Awards No. 1912350 and No. 2207977. We thank Jia Wang and Jose D'Incao for sharing their computer programs.

[1] S. Inouye, M. Andrews, J. Stenger, H.-J. Miesner, D. M. Stamper-Kurn, and W. Ketterle, Observation of Feshbach resonances in a Bose–Einstein condensate, Nature (London) **392**, 151 (1998).

[2] V. Efimov, Energy levels arising from resonant two-body forces in a three-body system, Phys. Lett. B **33**, 563 (1970).

[3] V. Efimov, Weakly-bound states of three resonantly interacting particles, Sov. J. Nucl. Phys. **12**, 589 (1971) [Yad. Fiz. **12**, 1080 (1970)].

[4] E. Braaten and H.-W. Hammer, Universality in few-body systems with large scattering length, Phys. Rep. **428**, 259 (2006).

[5] Y. Wang, J. P. D'Incao, and B. D. Esry, Chapter 1 - ultracold few-body systems, in *Advances in Atomic, Molecular, and Optical Physics*, edited by E. Arimondo, P. R. Berman, and C. C. Lin, Advances in Atomic, Molecular, and Optical Physics Vol. 62 (Academic Press, New York, 2013), pp. 1–115.

[6] P. Naidon and S. Endo, Efimov physics: A review, Rep. Prog. Phys. **80**, 056001 (2017).

[7] J. P. D'Incao, Few-body physics in resonantly interacting ultracold quantum gases, J. Phys. B: At., Mol. Opt. Phys. **51**, 043001 (2018).

[8] H. Suno, B. D. Esry, C. H. Greene, and J. P. Burke, Three-body recombination of cold helium atoms, Phys. Rev. A **65**, 042725 (2002).

[9] M. Kunitski, S. Zeller, J. Voigtsberger, A. Kalinin, L. P. H. Schmidt, M. Schöffler, A. Czasch, W. Schöllkopf, R. E. Grisenti, T. Jahnke *et al.*, Observation of the Efimov state of the helium trimer, Science **348**, 551 (2015).

[10] T. Kraemer, M. Mark, P. Waldburger, J. G. Danzl, C. Chin, B. Engeser, A. D. Lange, K. Pilch, A. Jaakkola, H.-C. Nägerl *et al.*, Evidence for Efimov quantum states in an ultracold gas of caesium atoms, Nature (London) **440**, 315 (2006).

[11] M. Berninger, A. Zenesini, B. Huang, W. Harm, H.-C. Nägerl, F. Ferlaino, R. Grimm, P. S. Julienne, and J. M. Hutson, Universality of the Three-Body Parameter for Efimov States in Ultracold Cesium, Phys. Rev. Lett. **107**, 120401 (2011).

[12] M. Zaccanti, B. Deissler, C. D'Errico, M. Fattori, M. Jona-Lasinio, S. Müller, G. Roati, M. Inguscio, and G. Modugno, Observation of an Efimov spectrum in an atomic system, Nat. Phys. **5**, 586 (2009).

[13] S. E. Pollack, D. Dries, and R. G. Hulet, Universality in three- and four-body bound states of ultracold atoms, Science **326**, 1683 (2009).

[14] N. Gross, Z. Shotan, S. Kokkelmans, and L. Khaykovich, Observation of Universality in Ultracold ^{7}Li Three-Body Recombination, Phys. Rev. Lett. **103**, 163202 (2009).

[15] T. B. Ottenstein, T. Lompe, M. Kohnen, A. N. Wenz, and S. Jochim, Collisional Stability of a Three-Component Degenerate Fermi Gas, Phys. Rev. Lett. **101**, 203202 (2008).

[16] R. J. Wild, P. Makotyn, J. M. Pino, E. A. Cornell, and D. S. Jin, Measurements of Tan's Contact in an Atomic Bose-Einstein Condensate, Phys. Rev. Lett. **108**, 145305 (2012).

[17] B. D. Esry, C. H. Greene, and J. P. Burke, Recombination of Three Atoms in the Ultracold Limit, Phys. Rev. Lett. **83**, 1751 (1999).

[18] J. H. Macek and J. Sternberg, Properties of Pseudopotentials for Higher Partial Waves, Phys. Rev. Lett. **97**, 023201 (2006).

[19] E. Braaten, P. Hagen, H.-W. Hammer, and L. Platter, Renormalization in the three-body problem with resonant *p*-wave interactions, Phys. Rev. A **86**, 012711 (2012).

[20] Y. Nishida, Impossibility of the Efimov effect for *p*-wave interactions, Phys. Rev. A **86**, 012710 (2012).

[21] Y. Nishida and S. Tan, Liberating Efimov physics from three dimensions, Few-Body Syst. **51**, 191 (2011).

[22] Y.-H. Chen and C. H. Greene, Efimov physics implications at *p*-wave fermionic unitarity, Phys. Rev. A **105**, 013308 (2022).

[23] O. I. Kartavtsev and A. V. Malykh, Low-energy three-body dynamics in binary quantum gases, J. Phys. B: At., Mol. Opt. Phys. **40**, 1429 (2007).

[24] P. Naidon, L. Pricoupenko, and C. Schmickler, Shallow trimers of two identical fermions and one particle in resonant regimes, SciPost Phys. **12**, 185 (2022).

[25] M. D. Higgins and C. H. Greene, Three and four identical fermions near the unitary limit, Phys. Rev. A **106**, 023304 (2022).

[26] X. Du, Y. Zhang, and J. E. Thomas, Inelastic Collisions of a Fermi Gas in the BEC-BCS Crossover, Phys. Rev. Lett. **102**, 250402 (2009).

[27] J. P. D'Incao and B. D. Esry, Scattering Length Scaling Laws for Ultracold Three-Body Collisions, Phys. Rev. Lett. **94**, 213201 (2005).

[28] D. S. Petrov, Three-body problem in Fermi gases with short-range interparticle interaction, Phys. Rev. A **67**, 010703(R) (2003).

[29] B. D. Esry, C. H. Greene, and H. Suno, Threshold laws for three-body recombination, Phys. Rev. A **65**, 010705(R) (2001).

[30] S. T. Rittenhouse, J. von Stecher, J. P. D'Incao, N. P. Mehta, and C. H. Greene, The hyperspherical four-fermion problem, J. Phys. B: At., Mol. Opt. Phys. **44**, 172001 (2011).

[31] C. H. Greene, P. Giannakeas, and J. Pérez-Ríos, Universal few-body physics and cluster formation, Rev. Mod. Phys. **89**, 035006 (2017).

[32] R. C. Whitten and F. T. Smith, Symmetric representation for three body problems. II. Motion in space, J. Math. Phys. **9**, 1103 (1968).

[33] B. R. Johnson, On hyperspherical coordinates and mapping the internal configurations of a three body system, J. Chem. Phys. **73**, 5051 (1980).

[34] B. K. Kendrick, R. T. Pack, R. B. Walker, and E. F. Hayes, Hyperspherical surface functions for nonzero total angular momentum. I. Eckart singularities, J. Chem. Phys. **110**, 6673 (1999), https://doi.org/10.1063/1.478574.

[35] J. Wang, J. P. D'Incao, B. D. Esry, and C. H. Greene, Origin of the Three-Body Parameter Universality in Efimov Physics, Phys. Rev. Lett. **108**, 263001 (2012).

[36] N. P. Mehta, S. T. Rittenhouse, J. P. D'Incao, J. von Stecher, and C. H. Greene, General Theoretical Description of *n*-Body Recombination, Phys. Rev. Lett. **103**, 153201 (2009).

[37] J. Wang, J. P. D'Incao, and C. H. Greene, Numerical study of three-body recombination for systems with many bound states, Phys. Rev. A **84**, 052721 (2011).

[38] F. Werner and Y. Castin, Unitary Quantum Three-Body Problem in a Harmonic Trap, Phys. Rev. Lett. **97**, 150401 (2006).

[39] D. Blume, J. von Stecher, and C. H. Greene, Universal Properties of a Trapped Two-Component Fermi Gas at Unitarity, Phys. Rev. Lett. **99**, 233201 (2007).

[40] H. Suno, B. D. Esry, and C. H. Greene, Recombination of Three Ultracold Fermionic Atoms, Phys. Rev. Lett. **90**, 053202 (2003).

[41] Y. Wang, Multi-photon ionization studies of correlation effects in excited atoms, Ph.D. thesis, Purdue University Graduate School, 2022.

[42] C. Chin, R. Grimm, P. Julienne, and E. Tiesinga, Feshbach resonances in ultracold gases, Rev. Mod. Phys. **82**, 1225 (2010).

[43] V. V. Flambaum, G. F. Gribakin, and C. Harabati, Analytical calculation of cold-atom scattering, Phys. Rev. A **59**, 1998 (1999).

[44] M. V. Berry, Semi-classical scattering phase shifts in the presence of metastable states, Proc. Phys. Soc. **88**, 285 (1966).

[45] C. W. Clark, The calculation of non-adiabatic transition probabilities, Phys. Lett. A **70**, 295 (1979).

[46] H. R. Sadeghpour, J. L. Bohn, M. J. Cavagnero, B. D. Esry, I. I. Fabrikant, J. H. Macek, and A. Rau, Collisions near threshold in atomic and molecular physics, J. Phys. B: At. Mol. Opt. Phys. **33**, R93 (2000).